Available online at www.sciencedirect.com

ScienceDirect

Procedia Manufacturing 26 (2018) 712–719

Procedia MANUFACTURING

www.elsevier.com/locate/procedia

46th SME North American Manufacturing Research Conference, NAMRC 46, Texas, USA

Nd^{3+}:YAG laser surface processing of moly-chrome film at 1064 nm, 532 nm and 355 nm wavelengths

V. Ezhilmaran[a,*], L. Vijayaraghavan[a], N. J. Vasa[b]

[a]*Department of Mechanical Engineering, Indian Institute of Technology Madras, Chennai-600036, INDIA*
[b]*Department of Engineering Design, Indian Institute of Technology Madras, Chennai-600036, INDIA*

* Corresponding author. Tel.: +91-9840345256
E-mail address: me13d062@smail.iitm.ac.in

Abstract

A nanosecond pulsed Nd^{3+}:YAG laser was used to generate grooves as well as dimples on the surface of the moly-chrome film. Interaction of laser, operating at the laser wavelengths of 1064 nm, 532 nm and 355 nm, respectively on the target material were investigated. The principal finding is based on the geometrical parameters such as width, depth and recast layer in the case of the groove. Various roughness parameters inside the grooves were studied. Whereas in the case of the dimple, various parameters like dimple diameter, depth and recast laser were analyzed. A study to find the optical reflectivity of the moly-chrome material at different laser wavelengths was conducted. The groove and dimple formed with the laser wavelength of 1064 nm showed a high material removal and re-cast layer compared to 532 nm and 355 nm. The roughness R_a inside the groove formed with the laser wavelength of 1064 nm and 355 nm exhibited a percentage increase of around 68% and 20% compared to the 532 nm.

Peer-review under responsibility of the scientific committee of the 46th SME North American Manufacturing Research Conference.

Keywords: Laser; Surface texture; Wavelength; Dimple; Groove.

1. Introduction

Micro-dimple formation on piston rings, cylinder liners and bearings can assist in storing oil. This approach can reduce friction wear and improve the engine tribology and life of automotive components. Laser-assisted texturing of such components has various advantages, such as flexibility in control of texture size, can be used for treating a wider range of materials with less heat affected zone, the absence of tool-workpiece contact, high processing speed and ability to obtain high dimensional precision. In particular, Nd^{3+}:YAG laser operating in a pulsed mode can also be considered for such texturing

2351-9789
Peer-review under responsibility of the scientific committee of the 46th SME North American Manufacturing Research Conference.
10.1016/j.promfg.2018.07.081

application because of large peak power and short pulse width resulting in narrow heat affected zone. Laser material processing is a method of ablating the target with a high-intensity laser beam [1]. It can also process almost any kind of materials irrespective of their material properties, such as hardness, toughness and thermal conductivity, etc. [2]. Laser-aided material processing has been reported on a variety of materials which include metals [3], ceramics [4] and polymers [5]. Laser ablation of metals is always accompanied by a change in surface and metallurgical properties, such as roughness, residual stress, phase transformation, etc. [6-9]. Many experimental investigations have been performed to study the effect of laser parameters, such as pulse duration, laser energy, pulse repetition rate [10], pulse duration [11], wavelength [12] and beam shape on the performance parameters such as ablation diameter and depth, material removal rate, dimensional accuracy and ablation quality. Laser wavelength and pulse duration play a key role in affecting the accuracy of laser processed surface [13, 14]. Amer et al. [15] reported that short pulsed lasers in the order of few nanoseconds to few microseconds induce substantial heat affected region during the laser-material interaction. Similarly, the influence of laser wavelength operating in near-IR/visible/UV region on material processing is also of high interest while using nanosecond pulsed Nd^{3+}:YAG laser [12]. Owing to the shorter wavelengths compared to CO_2 laser, Nd^{3+}: YAG laser could process even finely polished metallic surfaces with ease [16]. In the case of Nd^{3+}: YAG laser, laser surface processing is mostly carried out by using a pulsed laser with a wavelength around 1064 nm and pulse width ranging around few hundred nanoseconds. Vilhena et al. [17] used Nd^{3+}:YAG pulsed laser with a power of up to 80 W, the wavelength of 1064 nm and pulse duration varying from 98 to 597 ns to produce dimples on 100Cr6 steel plates. Their study showed that with a single-mode Gaussian pulse, accurate processing of the material with small thermal damages was noticed for short pulse duration. Greiner et al. [18] used Q-switched Ytterbium-doped fiber laser with a power of up to 20 W and a wavelength of 1064 nm to create various micro-dimple patterns on the flat portion of the spherical CuZn36 alloy brass material. Most of the studies reported so far, utilizes fundamental wavelength of 1064 with a pulse width ranging from a hundred to few hundred of nanoseconds [19]. On the other hand, laser pulses of shorter wavelength can also be considered for material processing application, as the heat defects were expected to be less. Hence, it is necessary to use the appropriate laser parameters, such as the wavelength that can offer minimal thermal defects.

In this work, nanosecond pulsed Nd^{3+}:YAG laser is used to ablate moly-chromium deposited (film thickness: 130 µm) cast iron piston ring. This work attempts to analyze the size and depth of the grooves and dimples formed with the laser wavelengths of 355 nm, 532 nm and 1064 nm, respectively. The geometrical parameters of the grooves and the dimples were investigated. Also, the ablation quality for different laser wavelength was analyzed by measuring the size of recast layer. Furthermore, roughness inside the groove formed with different wavelengths was investigated.

2. Experimental details

The target material was commercially available piston ring. The ring made from the spheroidal graphite cast iron piston ring consisted of a moly-chrome thin film coating (Cr - 94%, O - 5.5%, Al - 0.2%, Mo - 0.2% and B - 0.1%) of thickness 130 µm. The ring has an inner diameter of 89 mm, width of 2.4 mm and thickness of 3 mm. The hardness of the moly-chrome film was measured to be 940 HV. A nanosecond pulsed Nd^{3+}:YAG laser with pulse duration of 6 ns and pulse repetition rate of 10 Hz was used to produce groove and dimple texture on the moly-chrome film. Various laser parameters used in the present study is shown in Table 1. A 300-mm biconvex lens was used to focus a near-Gaussian laser beam profile. All the samples were ablated at the focal position. Figure 1 shows the ring sample mounted on a rotary stage (Sigma Koki shot, Mini 5P) that was fixed to XY translational stage. The

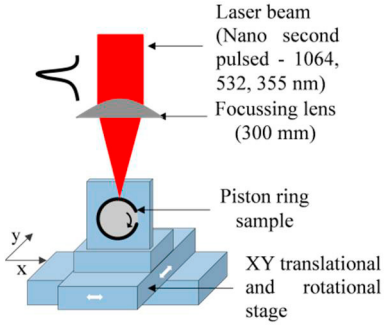

Fig. 1 Experimental setup for laser surface processing.

material was irradiated with three different wavelengths, such as 1064 nm, 532 nm and 355 nm, respectively to produce dimple and groove texture. Laser pulse energy of 10 mJ was applied in all the cases. To produce grooves, the pulse overlap and number of laser passes were set at 90% and 4. Similarly, to produce dimples number of laser pulses of 25 was applied in each spot. The spacing between the grooves and dimples was set at 220 µm. The dimensions of the laser processed region were evaluated using the optical surface profiler (Bruker, Contour GT). The average depth was estimated by sampling at 10 different locations inside the groove and dimple and the average value was taken. The diameter of the dimple was measured along the material surface to eliminate the influence of recast layer during measurement. Scanning electron microscopy (FEI, Quanta 200) was used to examine the quality of the ablated surface.

Table 1 General laser parameters

Laser parameters	
Laser type	Nanosecond pulsed Nd^{3+}:YAG
Pulse repetition rate	10 Hz
Pulse duration	6 ns
Wavelength	1064 nm, 532 nm and 355 nm
Pulse energy (Grooves and dimples)	10 mJ
Number of passes (Grooves)	4
Pulse overlap (Grooves)	90%
Number of pulses (Dimples)	25

3. Results and discussion

3.1. Analysis of geometrical parameters of grooves

In order to find the influence of wavelength on the groove geometrical parameters, different samples were produced with the wavelengths of 1064 nm, 532 nm and 355 nm, respectively. Figure 2(a) shows the 3-D surface topography of the groove textured surface formed with the laser wavelength of 1064

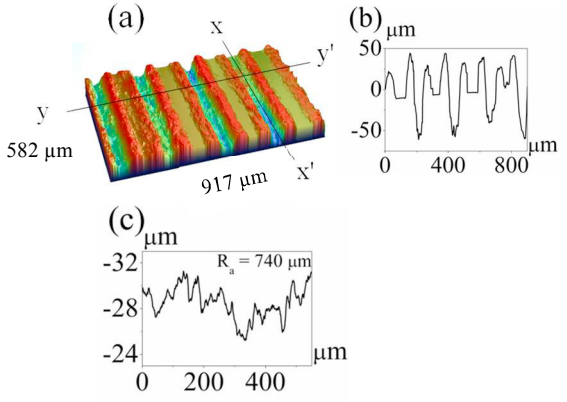

Fig. 2(a) 3D surface of the groove textured ring formed with λ = 1064 nm, (b) Corresponding surface profile of grooves along y-y' axis and (c) Corresponding roughness inside the groove along x-x' axis.

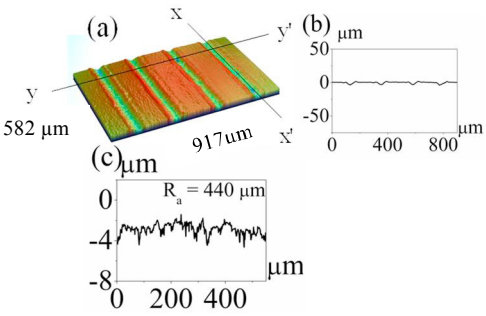

Fig. 3(a) 3D surface of the groove textured ring formed with λ = 532 nm, (b) Corresponding surface profile of grooves along y-y' axis and (c) Corresponding roughness inside the groove along x-x' axis.

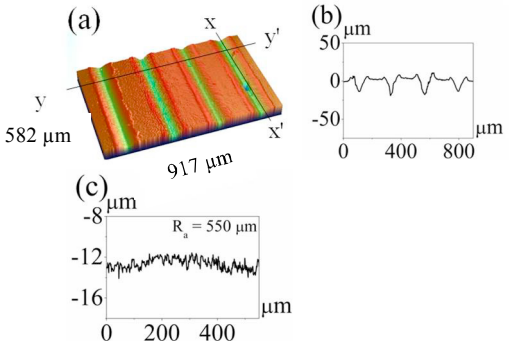

Fig. 4(a) 3D surface of the groove textured ring formed with λ = 355 nm, (b) Corresponding surface profile of grooves along y-y' axis and (c) Corresponding roughness inside the groove along x-x' axis.

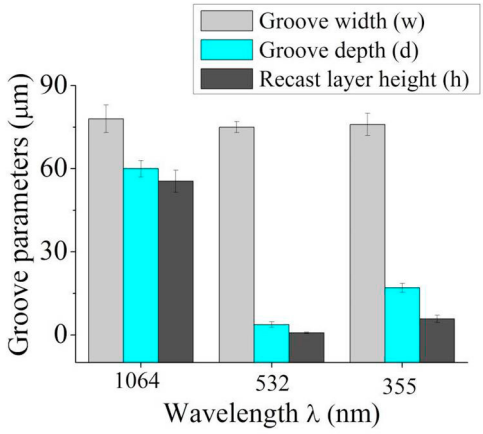

Fig. 5 Variation of groove parameters as a function of laser wavelength.

nm. The surface profile along y-y' is shown in Fig. 2(b). The groove is very deep with a large amount of recast layer pile-up around the groove edge. Figure 2(c) shows that the surface inside the groove along x-x' axis was very rough. The 3-D groove textured surface formed using the laser wavelength of 532 nm is shown in Fig. 3(a). Though the same energy was used to form the grooves, the depth of the groove and roughness inside the groove decreased (Fig. 3(b, c)) compared to 1064 nm. Figure 4(a) shows the 3-D surface topography of the grooves formed with the laser wavelength of 355 nm. The groove depth was increased compared to 532 nm and decreased compared to 1064 nm (Fig. 4(b)). At the same time, roughness was decreased compared to 532 nm and 1064 nm (Fig. 4(c)). Figure 5 shows the variation of groove parameters such as groove width, depth and recast layer as a function of laser wavelength. The groove width was almost same for the grooves formed with all the laser wavelengths and hence the change in groove width was assumed insignificant. But a significant difference in groove depth and recast layer height was observed. A groove depth of around 60 µm was observed with the laser wavelength of 1064 nm for the laser pulse energy of 10 mJ and 25 number of pulses. A groove depth of around 17 µm was obtained with the wavelength of 355 nm for the same pulse energy and number of pulses. For the laser wavelength of 532 nm, the lowest groove depth of around 4 µm was observed. Hence, the aspect ratio which is defined as the ratio of groove width (w) and depth (d) was less with the laser wavelength of 532 nm (0.05) compared to the remaining wavelengths as shown in Fig. 6. A high aspect ratio of around 0.76 was observed with the laser wavelength of 1064 nm.

Previous studies performed by Johnson et al. showed that the absorption coefficient (α) of chromium with 1064 nm (4.2×10^5 cm^{-1}) is less compared to 355 nm ($\alpha = 9.4\times10^5$ cm^{-1}) and 532 nm (7.8×10^5 cm^{-1}) [20]. Hence, the laser penetration depth which is the inverse of absorption coefficient was expected to be high for 1064 nm as compared to 532 nm and 355 nm. This verified that the material removal might be mostly due to melt ejection while using the laser wavelength of 1064 nm. This might have resulted in high metal removal, in the laser ablated region while using the laser wavelength of 1064 nm as compared to 532 nm and 355 nm [21]. Moreover, the ejected molten materials and the plasma that was formed in front of the sample were more easily penetrated by 1064 nm beam compared to 532 nm beam [22]. Though the absorption coefficient of the material with the wavelength of 355 nm is the least compared to 532 nm, the lowest material removal was observed with 532 nm. This might be attributed to a change in optical reflectivity from the target surface while using different wavelengths.

In order to understand the influence of laser wavelength on the recast layer formation, the term h/d was plotted as a function of laser wavelength as shown in Fig. 7. Where 'h' represents the recast layer height and 'd' represents the depth of the ablated portion. A high h/d ratio was observed in the groove fabricated with the laser wavelength of 1064 nm, followed by 355 nm and 532 nm.

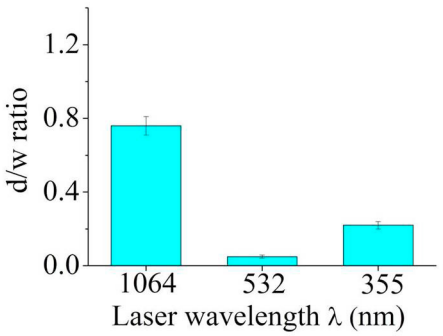

Fig. 6 Influence of laser wavelength on d/w ratio of the groove. d: Groove depth and w: Groove width.

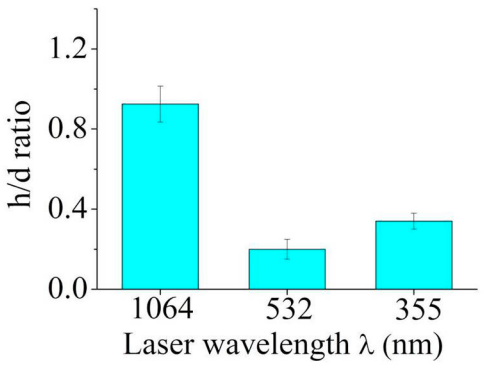

Fig. 7 Influence of laser wavelength on h/d ratio of the groove. h: Recast layer height and d: Groove depth.

The less h/d ratio with 532 nm and 355 nm shows that the material removal might be due to the combined effect of melting and vaporization. Hence, some of the material removed from the substrate might be vaporized instead of getting piled up around the groove edge. Figure 8 shows the roughness

parameters, such as R_a, R_q and R_t inside the grooves was substantially high with 1064 nm, compared to other wavelengths. The roughness R_a inside the groove formed with the laser wavelength of 1064 nm and 355 nm exhibited an increase in roughness of around 68% and 20% compared to the 532 nm. This shows that the roughness increases with the increase of material removal. In the case of groove fabricated with the laser wavelength of 1064 nm, a certain portion of melt remained inside the groove which is attributed to the reason for the increase in roughness inside the groove.

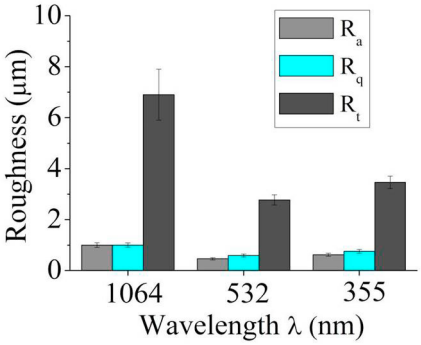

Fig. 8 Variation of roughness inside the groove as a function of laser wavelength.

3.2 Analysis of geometrical parameters of dimples

Figure 9(a) to (c) shows the 3D surface topography of the dimple textured surface formed using the laser wavelength of 1064 nm, 532 nm and 355 nm, respectively. All the dimples located in the different samples were fabricated using the laser with pulse energy of 5 mJ and 25 number of pulses. Figure

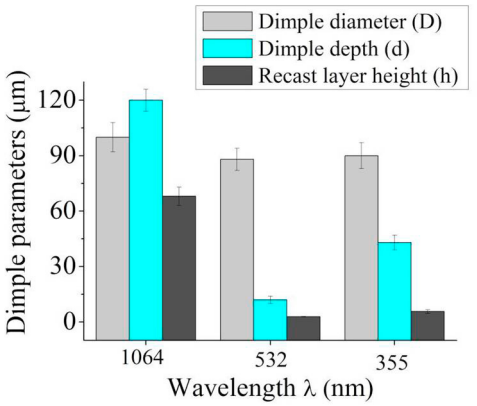

Fig. 10 Variation of dimple parameters as a function of laser wavelength.

9(d) to (f) shows the corresponding surface profile of the textured samples obtained with the laser wavelength of 1064 nm, 532 nm and 355 nm, respectively. Similar to the grooves, the dimple depth and the recast layer formed around the dimple fabricated with the laser wavelength of 1064 nm was high compared to 532 nm and 355 nm (Fig. 10). The change in dimple diameter was very small as that of the groove. As the number of pulses to irradiate the sample at a particular location was relatively higher compared to the grooves, the depth of the dimples was high compared to groove. A high dimple aspect ratio of around 1.2 was observed with the wavelength of 1064 nm as shown in Fig. 11. For the wavelength of 355 nm and 532 nm, the dimple aspect ratio was notably reduced. Though the aspect ratio increased in the dimple, the recast layer height was reduced

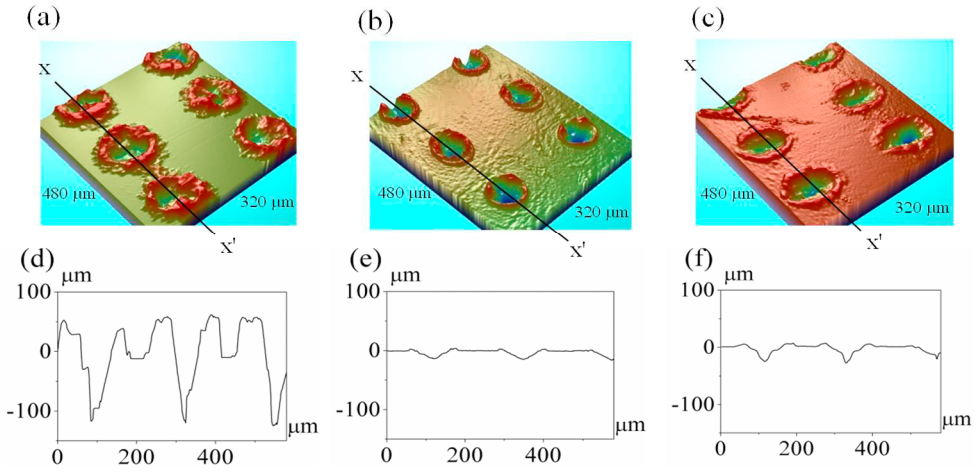

Fig. 9 3D surface of the dimple textured ring formed with the wavelength of (a) 1064 nm, (b) 532 nm and (c) 355 nm. Corresponding surface profile of the dimple along x-x' axis for the wavelength of (d) 1064 nm, (e) 532 nm and (f) 355 nm.

compared to the groove. This is attributed to the flow of large amount melt piled up around the dimple edges. The h/d ratio of the dimple formed with 532 and 355 nm showed a relatively less value compared to 1064 nm (Fig. 12).

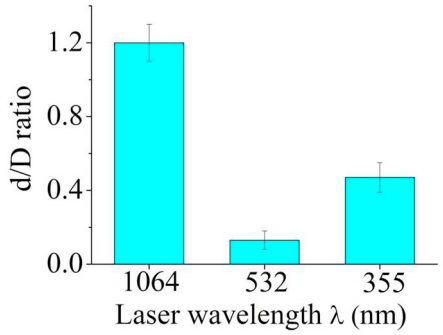

Fig.11 Influence of laser wavelength on d/D ratio of the dimple d: Dimple depth and D: Dimple diameter.

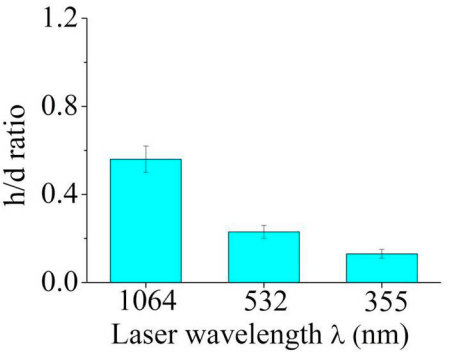

Fig. 12 Influence of laser wavelength on h/d ratio of the dimple. h: Recast layer height and d: Dimple depth.

3.3 Optical reflectivity measurement

In order to understand the laser-material interaction behavior, the reflectivity of the material was measured for all the wavelengths considered for the analysis. Appropriate aperture size was used to maintain the laser beam diameter at 1 mm, so as to ensure that the beam falls within the material surface. A portion of the incident laser beam reflected from the moly-chrome material surface was measured by using a power meter. The reflectivity measurement was carried out at different laser fluence below the ablation threshold as shown in Fig. 13. The average reflectivity was estimated by taking the mean of all reflectivity values. The reflectivity of moly-chrome material for 1064 nm, 532 nm and 355 nm was measured as ≈46%, ≈36% and ≈20%, respectively. Experiments were performed multiple times and average reflectivity values were estimated. As the reflectivity of the material at 355 nm was less, energy coupling between the laser and the material surface might be high with 355 nm compared to other wavelengths.

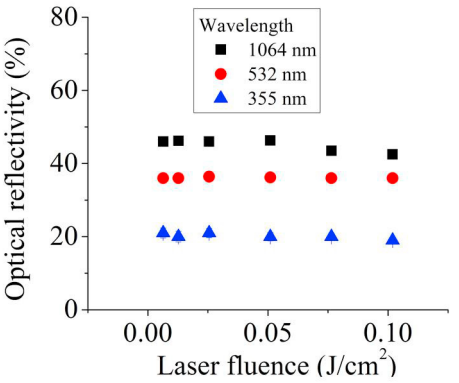

Fig. 13 Optical reflectivity of moly-chrome material as a function of laser fluence for the laser wavelengths of 1064 nm, 532 nm and 355 nm.

On the other hand, the laser ablation depth and diameter formed using the laser wavelength of 532 nm was less compared to the remaining wavelengths. The might be due to the influence of absorption coefficient of the target material which varies for different wavelengths. The moly-chrome ceramic mainly contains chromium as a major composition. The study performed by Johnson et al. showed that the absorption coefficient (α) of chromium with 355 nm ($\alpha = 9.4 \times 10^5$ cm^{-1}) was less compared to 532 nm (7.8×10^5 cm^{-1}) and 1064 nm (4.2×10^5 cm^{-1}) [20]. However, no previous literature are found to study the optical absorption coefficient of the moly-chrome ceramic alloy. The optical absorption coefficient of moly-chrome ceramic for the wavelength of 532 nm is expected to be high compared to 355 nm and 1064 nm. Hence, the penetration depth might be less for the laser wavelength of 532 nm. Further studies are carried out to find the absorption coefficient of the moly-chrome material by an appropriate method.

3.4 SEM analysis

Figure 14(a) to (c) shows the SEM image of the groove fabricated with the laser wavelength of 1064 nm, 532 nm and 355 nm, respectively. The SEM image of the dimple formed with the laser wavelength of 1064 nm, 532 nm and 355 nm,

respectively is shown in Fig. 13(d) to (f). The EDS analysis was carried out in the recast layer. The common elements present in all the spots were Cr, Mo, C, O and Al respectively as shown in Table 2. The target material mainly consisted of chromium (Cr > 93%) balanced by other elements to 100 %. The elemental analysis at the recast layer is shown in Table 2. The notations G and D were used to represent groove and dimple (see Table 2). The results showed that the oxygen and carbon percentage was high in the recast layer, formed with the wavelength of 1064 nm. This is attributed to a high

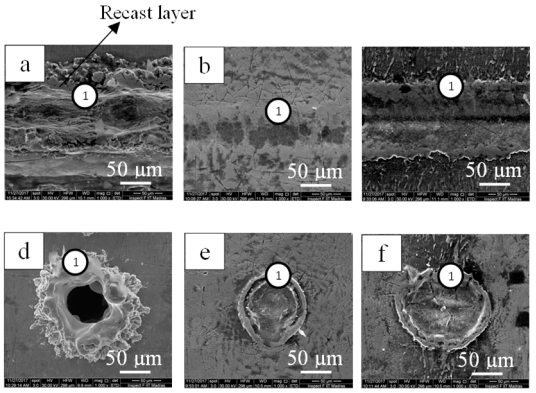

Fig. 14 SEM image of the groove formed with the wavelength of (a) 1064 nm, (b) 532 nm and (c) 355 nm & SEM image of the dimple formed with the wavelength of (a) 1064 nm, (b) 532 nm and (c) 355 nm.

Table 2 EDAX analysis at the recast layer.

Sample	Elements weight percentage (%)			
	Cr	C	O	Mo
G-1064 nm	54	24	18	0.1
G-532 nm	84	7	6	0.1
G-355 nm	73	11	12	0.1
D-1064 nm	50	28	18	0.2
D-532 nm	80	9	8	0.1
D-355 nm	72	15	11	0.2
Moly-Chrome	94	-	5.5	0.2

magnitude of melting at the target during irradiation with 1064 nm. This melt could easily interact with the carbon and oxygen in the atmosphere resulted in an increase in carbon and oxygen concentration. At the same time, both groove and dimple formed with the wavelength of 532 nm showed less carbon and oxygen concentration.

4. Conclusion

The laser ablation experiments were performed on the moly-chrome film using nanosecond pulsed Nd^{3+}:YAG laser. Grooves and dimples were produced on the target material with the laser wavelengths of 1064 nm, 532 nm and 355 nm, respectively. The material removal and the corresponding recast layer formation were high with the laser wavelength of 1064 nm in the case of both grooves and dimples. The roughness inside the grooves was high in the sample fabricated with 1064 nm. The laser wavelength of 532 nm offered low material removal and recast layer with a low surface roughness inside the grooves. Dimples showed the same phenomena as that of the grooves for all the wavelengths in terms of geometrical and metallurgical properties. Further studies are carried out to study the absorption coefficient and the residual stress induced on the laser textured surface formed with different wavelengths.

Acknowledgements

The authors would like to thank Dr. Mahadevan of India pistons limited for their continuous support. The authors also wish to thank Mr. Jeyakumar of MEMS lab, IIT Madras for his help in characterization of the samples. The research work is supported by DST-AMT Program (DST/TSG/AMT/2015/353).

Reference

[1] A.K. Dubey, V. Yadava, Laser beam machining—A review, International Journal of Machine Tools and Manufacture, 48 (2008) 609-628.
[2] S.S. Singh, P.K. Baruah, A. Khare, S.N. Joshi, Effect of laser beam conditioning on fabrication of clean micro-channel on stainless steel 316L using second harmonic of Q-switched Nd: YAG laser, Optics & Laser Technology, 99 (2018) 107-117.
[3] R. Jordan, D. Cole, J.G. Lunney, K. Mackay, D. Givord, Pulsed laser ablation of copper, Applied Surface Science, 86 (1995) 24-28.
[4] T.V. Kononenko, S.V. Garnov, S.M. Klimentov, V.I. Konov, E.N. Loubnin, F. Dausinger, A. Raiber, C. Taut, Laser ablation of metals and ceramics in picosecond–nanosecond pulse width in the presence of different ambient atmospheres, Applied Surface Science, 109-110 (1997) 48-51.
[5] A.A. Serafetinides, M.I. Makropoulou, C.D. Skordoulis, A.K. Kar, Ultra-short pulsed laser ablation of polymers, Applied Surface Science, 180 (2001) 42-56.
[6] J. Zhao, Y. Dong, C. Ye, Laser shock peening induced residual stresses and the effect on crack propagation behavior, International Journal of Fatigue, 100 (2017) 407-417.

[7] Y. Jiang, X. Xiang, C.M. Liu, H.J. Wang, W. Liao, H.B. Lv, X.D. Yuan, R. Qiu, Y.J. Yang, W.G. Zheng, X.T. Zu, Effect of residual stress on laser-induced damage characterization of mitigated damage sites in fused silica, Journal of Non-Crystalline Solids, 410 (2015) 88-95.
[8] Y. Zhang, L. Liu, G. Zou, N. Chen, A. Wu, H. Bai, Y. Zhou, Femtosecond laser-induced phase transformations in amorphous Cu77Ni6Sn10P7 alloy, Journal of Applied Physics, 117 (2015) 023109.
[9] I. Choi, H.Y. Jeong, H. Shin, G. Kang, M. Byun, H. Kim, A.M. Chitu, J.S. Im, R.S. Ruoff, S.-Y. Choi, Laser-induced phase separation of silicon carbide, Nature communications, 7 (2016) 13562.
[10] F. Burns, S.R. Cain, The effect of pulse repetition rate on laser ablation of polyimide and polymethylmethacrylate-based polymers, Journal of Physics D: Applied Physics, 29 (1996) 1349.
[11] B. Lauer, B. Jäggi, B. Neuenschwander, Influence of the Pulse Duration onto the Material Removal Rate and Machining Quality for Different Types of Steel, Physics Procedia, 56 (2014) 963-972.
[12] L. Tunna, A. Kearns, W. O'neill, C. Sutcliffe, Micromachining of copper using Nd: YAG laser radiation at 1064, 532, and 355 nm wavelengths, Optics & Laser Technology, 33 (2001) 135-143.
[13] J. Stasic, M. Trtica, B. Gakovic, D. Batani, T. Desai, G. Brankovic, Modifications of AISI 1045 steel by picosecond Nd: YAG laser at 266nm; comparison with 532 and 1064nm pulses, Applied Surface Science, 255 (2009) 8221-8225.
[14] B. Jaeggi, B. Neuenschwander, M. Schmid, M. Muralt, J. Zuercher, U. Hunziker, Influence of the pulse duration in the ps-regime on the ablation efficiency of metals, Physics Procedia, 12 (2011) 164-171.
[15] M.S. Amer, M.A. El-Ashry, L.R. Dosser, K.E. Hix, J.F. Maguire, B. Irwin, Femtosecond versus nanosecond laser machining: comparison of induced stresses and structural changes in silicon wafers, Applied Surface Science, 242 (2005) 162-167.
[16] A. Sharma, V. Yadava, Experimental analysis of Nd-YAG laser cutting of sheet materials – A review, Optics & Laser Technology, 98 (2018) 264-280.
[17] L.M. Vilhena, M. Sedlaček, B. Podgornik, J. Vižintin, A. Babnik, J. Možina, Surface texturing by pulsed Nd:YAG laser, Tribology International, 42 (2009) 1496-1504.
[18] G. Christian, M. Tobias, B. Daniel, C. Andrea, M. Franco, Optimum dimple diameter for friction reduction with laser surface texturing: the effect of velocity gradient, Surface Topography: Metrology and Properties, 3 (2015) 044001.
[19] S. Rusu, A. Buzaianu, L. Ionel, D. Ursescu, D.G. Galusca, Titanium alloy nanosecond vs. femtosecond laser marking, Applied Surface Science, 259 (2012) 311-319.
[20] P. Johnson, R. Christy, Optical constants of transition metals: Ti, v, cr, mn, fe, co, ni, and pd, Physical Review B, 9 (1974) 5056.
[21] M.S. Brown, C.B. Arnold, Fundamentals of laser-material interaction and application to multiscale surface modification, Laser precision microfabrication, 135 (2010) 91-120.
[22] J. Stasic, M. Trtica, B. Gakovic, S. Petrovic, D. Batani, T. Desai, P. Panjan, Surface modifications of AISI 1045 steel created by high intensity 1064 and 532nm picosecond Nd:YAG laser pulses, Applied Surface Science, 255 (2009) 4474-4478.